Impact of α-synuclein pathology on transplanted hESC-derived dopaminergic neurons in a humanized α-synuclein rat model of PD

Deirdre B. Hoban[a,b], Shelby Shrigley[a,b], Bengt Mattsson[a], Ludivine S. Breger[c], Ulla Jarl[a], Tiago Cardoso[a,b], Jenny Nelander Wahlestedt[a,b], Kelvin C. Luk[d], Anders Björklund[a,c,1], and Malin Parmar[a,b,1]

[a]Developmental and Regenerative Neurobiology, Wallenberg Neuroscience Center, 22184 Lund University, Lund, Sweden; [b]Lund Stem Cell Center, 22184 Lund University, Lund, Sweden; [c]Neurobiology, Department of Experimental Medical Science, Lund University, 22184 Lund, Sweden; and [d]Center for Neurodegenerative Disease Research, Department of Pathology and Laboratory Medicine, University of Pennsylvania Perelman School of Medicine, Philadelphia, PA 19104

Contributed by Anders Björklund, May 6, 2020 (sent for review January 28, 2020; reviewed by Donato A. Di Monte and Su-Chun Zhang)

Preclinical assessment of the therapeutic potential of dopamine (DA) neuron replacement in Parkinson's disease (PD) has primarily been performed in the 6-hydroxydopamine toxin model. While this is a good model to assess graft function, it does not reflect the pathological features or progressive nature of the disease. In this study, we establish a humanized transplantation model of PD that better recapitulates the main disease features, obtained by coinjection of preformed human α-synuclein (α-syn) fibrils and adeno-associated virus (AAV) expressing human wild-type α-syn unilaterally into the rat substantia nigra (SN). This model gives rise to DA neuron dysfunction and progressive loss of DA neurons from the SN and terminals in the striatum, accompanied by extensive α-syn pathology and a prominent inflammatory response, making it an interesting and relevant model in which to examine long-term function and integrity of transplanted neurons in a PD-like brain. We transplanted DA neurons derived from human embryonic stem cells (hESCs) into the striatum and assessed their survival, growth, and function over 6 to 18 wk. We show that the transplanted cells, even in the presence of ongoing pathology, are capable of innervating the DA-depleted striatum. However, on closer examination of the grafts, we found evidence of α-syn pathology in the form of inclusions of phosphorylated α-syn in a small fraction of the grafted DA neurons, indicating host-to-graft transfer of α-syn pathology, a phenomenon that has previously been observed in PD patients receiving fetal tissue grafts but has not been possible to demonstrate and study in toxin-based animal models.

Parkinson's disease | dopamine | pathology transfer | inflammation | disease modeling

The core pathology in Parkinson's disease (PD) involves loss of dopamine (DA) neurons in the substantia nigra (SN) and a consequent loss of the neurotransmitter DA in the striatum, resulting in the development of the characteristic motor symptoms of the disease. Because of this relatively focal degeneration, cell therapy aimed at replacing the lost DA neurons via transplantation has long been regarded as a promising treatment strategy. Initial proof-of-concept studies for this hypothesis were first performed in the late 1980s, with the transplantation of DA-rich fetal ventral mesencephalic (VM) tissue into PD patients (1, 2). While these studies provided evidence for the safety and efficacy of this strategy, a large variation in clinical outcome was observed (3). Given the limited access to human fetal tissue, the treatment has been hard to scale up, optimize, and standardize (4). In addition, use of tissues from aborted fetuses is ethically problematic and in some countries also prohibited, and there is a need to find an alternative and scalable source of DA neurons specifically designed for transplantation in PD patients. Recently, several protocols for the generation of transplantable and authentic DA neurons from human pluripotent stem cells (hPSCs) have been reported (5–12). The first clinical trials using induced pluripotent stem cell (iPSC)-derived cells have been initiated in Japan (13–15) and clinical trials with human embryonic stem cell (hESC)-derived DA neurons are currently being planned at multiple centers around the world (16).

The majority of preclinical validation studies used to assess the therapeutic potential of fetally and hPSC-derived DA neurons have been performed in the 6-hydroxydopamine (6-OHDA) rodent model or the 1-methyl-4-phenyl-1,2,3,6-tetrahydropyridine (MPTP) primate model of PD. These are toxin-induced models of acute DA neuron cell death which are suitable for assessing survival, maturation, DA release, and function of the transplanted cells. However, these models do not reflect the key pathological features or progressive nature of the human disease, and as such are not ideal to predict the effect of a pathological host environment on the survival, maturation, long-term functionality, and integrity of the cells in a diseased brain. As an example, analysis of post mortem tissue from patients transplanted with fetal VM tissue has revealed the presence of Lewy

Significance

Stem cell-based dopamine (DA) neuron replacement holds great potential for the treatment of Parkinson's disease (PD). Preclinical assessments have largely been limited to transplantation in the standard 6-hydroxydopamine toxin model of PD which does not reflect the pathological features of the disease. Here, we have developed and characterized an accelerated and humanized α-synuclein model of PD which better recapitulates the behavioral and pathological features of PD. We transplanted hESC-derived DA neurons in this model, finding they could survive, innervate, and integrate into host circuitry but that some grafted cells acquired the α-synuclein pathology at later time points. This has previously been observed in some patients who received fetally derived DA grafts but has thus far been difficult to model preclinically.

Author contributions: D.B.H., A.B., and M.P. designed research; D.B.H., S.S., B.M., L.S.B., U.J., T.C., and J.N.W. performed research; B.M. and K.C.L. contributed new reagents/analytic tools; D.B.H., S.S., A.B., and M.P. analyzed data; and D.B.H., A.B., and M.P. wrote the paper.

Reviewers: D.A.D.M., German Center for Neurodegenerative Diseases; and S.-C.Z., University of Wisconsin–Madison.

Competing interest statement: M.P. is the owner of Parmar Cells AB and coinventor on US patent application 15/093,927, owned by Biolamina AB, and EP17181588, owned by Miltenyi Biotec.

[1]To whom correspondence may be addressed. Email: anders.bjorklund@med.lu.se or malin.parmar@med.lu.se.

This article contains supporting information online at https://www.pnas.org/lookup/suppl/doi:10.1073/pnas.2001305117/-/DCSupplemental.

First published June 15, 2020.

body-like α-synuclein (α-syn) deposits in the grafted DA neurons appearing after an extended time period (>10 y) in some of the transplanted patients (17–23). The appearance of α-syn pathology in the grafted neurons has not been replicated in the toxin models, and therefore its potential impact on graft function has not been possible to assess experimentally.

In this study, we have sought to establish a novel, humanized transplantation model of PD that better mimics the disease pathology, including synucleinopathy, inflammation, motor impairment, and progressive DA neuron cell loss, to assess how a pathological host environment affects the transplanted cells and to allow for studies of potential host-to-graft transfer of pathology. The model is based on coinjection of human adeno-associated virus (AAV)-α-syn and human preformed α-syn fibrils (PFFs) which induces a rapid and prominent pathology in the host brain in a time frame suitable to assess the survival, integration, innervation, and function of transplanted hPSC-derived DA neurons in a "disease-like" brain. The progressive PD-like pathology seen in this model makes it an attractive complement to existing toxin-based models for predicting the clinical performance of transplanted DA neurons. Moreover, the key components of the model—overexpressed α-syn, PFFs, and grafted neurons—are all human, analogous to the patient brain environment, and thus provide a "humanized" system for studies. Using this model, we show that hESC-derived DA neurons transplanted to the striatum survive, integrate, and innervate the host striatum with a similar efficiency to parallel grafts in a partial 6-OHDA lesion model. At longer survival times, however, we observe cytoplasmatic deposits of phosphorylated α-syn (pSyn) in a fraction of the grafted DA neurons, suggesting host-to-graft triggering or transfer of pathology, as previously observed in some patients with fetal VM transplants (20, 22). Furthermore, we observe significant infiltration of microglia into the grafts, and the close apposition of activated microglia to affected DA neurons suggests that these cells may play an active role in this process.

Results

Progressive Cell Loss and Behavioral Deficits in Animals Simultaneously Injected with AAV-α-Synuclein and α-Synuclein Fibrils in the Substantia Nigra. Virally mediated overexpression of α-syn has emerged as a model of PD that mimics many of the pathological features (24–27). While virally mediated overexpression of α-syn produces relevant pathology in the rodent brain, the extent of DA neuron degeneration and resultant behavioral impairment is highly variable and takes a significant length of time to develop (28), which limits the model's usefulness for long-term neuroprotective and neurorestorative studies. In a previous study, Thakur et al. (29) have shown that PFFs can be used in combination with the AAV-α-syn vector to trigger PD-like pathology and DA neuron cell death. The sequential delivery of vector and PFFs with 3- to 4-wk intervals, as used by Thakur et al., demands, however, two separate surgical sessions, which is experimentally cumbersome and introduces an extra level of variability in the outcome. Thus, in order to more efficiently seed the propagation of pathology and accelerate the induction of pathology and cell loss, we combined AAV-mediated overexpression of human α-syn (at a level that alone does not cause overt degenerative effects) with delivery of human α-syn PFFs in a simultaneous injection to two sites in the SN (*SI Appendix*, Fig. S1).

Behavioral deficits were assessed in tests of both spontaneous and drug-induced motor behavior. Approximately 50% of animals in the group that received unilateral injections of both AAV-α-syn and PFFs (the SynFib animals) showed impairment in all three tests as early as 4 wk after administration (purple bars in Fig. 1 *A–C*) [stepping: $F_{(3,46)} = 28.37$, $P < 0.0001$; 4 wk: $^{****}t_{(46)} = 6.221$, $P < 0.0001$; 16 wk: $^{****}t_{(46)} = 5.941$, $P < 0.0001$; cylinder: $F_{(3,46)} = 3.015$, $^{*}P < 0.05$; rotation: $F_{(3,46)} = 28.37$, P = n.s. (not significant)]. The behavioral impairment in affected animals was sustained at 16 wk after injection, indicating a significant, stable, and measurable behavioral deficit in the SynFib-treated animals, while the animals in the AAV-α-syn–alone (aSyn) group showed only minor behavioral impairments at either 4- or 16-wk postinjection (red bars in Fig. 1 *A–C*).

Histological analysis confirmed that animals in the SynFib group had a significant loss of tyrosine hydroxylase (TH)-positive cell bodies in the SN of the injected side [$F_{(3,32)} = 19.19$, $P < 0.0001$, $^{**}t_{(32)} = 4.221$, $P = 0.0011$, $^{****}t_{(32)} = 5.369$, $P < 0.0001$] (Fig. 1 *D* and *F*), and a marked loss of TH+ fibers in the striatum (Fig. 1 *D* and *E*), which was much greater than in the aSyn-alone group, confirming the additive effect of coinjection of virus and PFFs for the induction of TH+ nigral cell loss. The presence of an early, measurable, and sustained behavioral phenotype in the SynFib model enables prescreening of the animals based on the behavioral tests in order to selectively intervene and follow these animals for long-term assessment of changes in motor function.

α-Syn Pathology and Nigral Cell Death Are Accompanied by Marked Inflammation along the Nigrostriatal Pathway. To further characterize the SynFib model, we studied the pathological changes induced by coinjection of AAV-α-syn and PFFs in comparison with the aSyn-alone control group. We first investigated the presence and pattern of the pathological form of α-syn by immunostaining using an antibody that detects the phosphorylated (at Ser129) form of the protein. In the aSyn–alone group of animals, we saw some degree of TH+ cell loss at 4 wk; however, minimal pSyn pathology was observed, both at the level of the SN (Fig. 2 *A* and *D* and *SI Appendix*, Fig. S2) and at the level of the striatum (Fig. 2*H*). In contrast, we found extensive pSyn pathology in SynFib-injected animals in the SN of the injected side (Fig. 2 *B* and *E*) and at the level of the ipsilateral but not contralateral striatum (Fig. 2 *I* and *L* and Movie S1) at 4 wk. These pSyn-positive cell bodies in the SN were TH-negative (Fig. 2*E′*). Given that the level of DA neuron degeneration reported in Fig. 1 was based on counting of TH+ cell bodies in the SN, the large number of TH−/pSyn+ cell bodies indicates that there is, in addition to acute cell loss, a certain level of TH down-regulation at this time point (Fig. 3). In comparison, when we examined the SynFib animals 16 wk after injection, we found many fewer neurons expressing pSyn+ pathology and an almost complete absence of TH+ cell bodies (Fig. 2 *C* and *F*). This suggests that the progress of α-syn–induced pathology occurs as follows: At early stages there is maximal development of pSyn+ inclusions and aggregates, and cells are clearly affected by the pathology given their loss of TH expression and the accompanying impairment in motor function. However, over time, most of the affected neurons have died, resulting in a loss of TH+ neurons and an overall reduction in cells expressing pSyn+ pathology (Fig. 2*E* versus Fig. 2*F*). This provides a time window where a therapeutic neuroprotective and disease-modifying intervention could be applied and assessed.

Next, we sought to examine the interplay between pathology and inflammation along the nigrostriatal pathway, as inflammation has been strongly implicated in the pathogenesis of PD (30). Minimal activation of Iba1+ microglia was present in the aSyn-alone group at 4 wk postinjection (Fig. 2*A*), whereas an aggravated microglial response (indicated by increased density and morphological changes) was clearly visible in the SynFib group at the same time point (Fig. 2*B*). The microglial cells were localized to areas of ongoing pathology (Fig. 2 *E* and *E′*) and some were found to surround and engulf the pSyn-positive cell bodies, seemingly attracted by the degenerating cells (Fig. 2*G* shows different examples of this). In the SynFib model at 16 wk, we found that the microglial response had returned to a level comparable to what was observed in the aSyn-alone animals at 4 wk (Fig. 2*C* vs. Fig. 2*A*), indicating that the active stage of pathology was complete at this stage (Fig. 2*F*). A similar pattern was observed at the

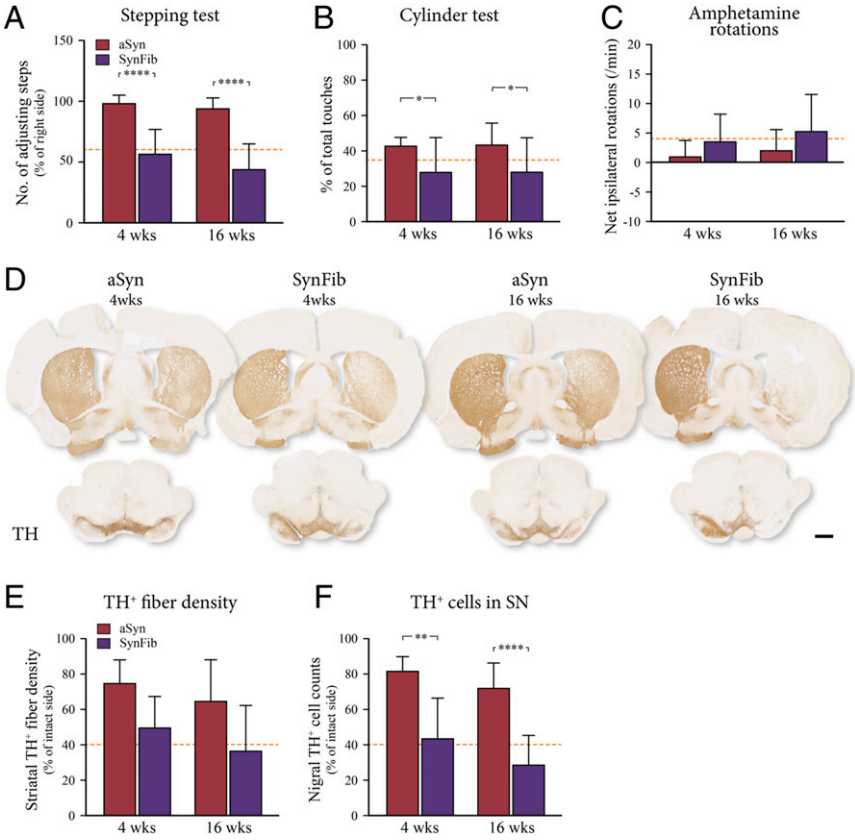

Fig. 1. Behavioral impairment and TH+ cell and fiber loss. aSyn and SynFib animals were assessed for behavioral impairment using the stepping test (*A*), cylinder test (*B*), and amphetamine-induced rotations (*C*) at both the 4- and 16-wk time points. All animals were immunohistochemically stained for TH to examine the integrity of the dopaminergic system (*D*). Quantification of TH+ fiber density in the striatum (*E*) and the number of TH+ cells in the SN (*F*) are expressed as a percentage of the contralateral side. Dotted lines in *A*, *B*, *E*, and *F* below the line indicate impairment/loss, whereas in *C* the impairment is above the line. All data are presented as mean ± SEM. $*P < 0.05$, $**P < 0.01$, $****P < 0.0001$, compared with the aSyn group at the same time point. (Scale bar, 1 mm.)

level of the striatum, where SynFib-injected animals after 4 wk exhibited a heightened level of microglial activation (Fig. 2*I*). Also, individual microglial cells were observed containing pSyn-positive inclusions, indicating either a direct transfer of seeding fibrillar material from the affected axons or active scavenging of degenerating axonal debris in the striatum (Fig. 2*K* shows different examples of this). This pathological and inflammatory environment of the striatum is of particular interest when utilizing this model in a cell-transplantation context, given that the most common site of transplantation of cells in preclinical PD models (and in patients) is ectopically in the striatum, where the endogenous DA fibers normally terminate.

At Early Time Points, Loss of TH Is Explained by a Combination of Cell Loss and Cellular Dysfunction Indicated by DA Marker Down-Regulation. The loss of TH immunoreactivity seen in nigral neurons with pSyn+ inclusions is in line with previous findings in the AAV-α-syn model and human PD showing that α-syn accumulation and aggregation are associated with a down-regulation of DA markers (31–33). At the level of the striatum, we found that there was a significant loss of TH+ fibers relative to the intact side (Figs. 1*D* and 3 *B*, *Inset*). At the early time point, 4 wk, we observed a small amount of α-syn–positive fibers and terminals that were TH-negative (Fig. 3 *A*–*C*; quantified in Fig. 3*G*), indicating down-regulation of TH in these fibers. We also found a number of striatal DA fibers that were double-positive for both TH and α-syn, indicating that they had been spared from the damage caused by excess α-syn (Fig. 3*A*). Additionally, we found that there were a number of TH+/α-syn− fibers, indicating that these were not targeted by the vector and therefore were unaffected by the pathology (Fig. 3*B*; quantified in Fig. 3*G*).

In the SN, the down-regulation seen at 4 wk in the pSyn+ neurons affected not only TH (quantified in Fig. 3*H*; visualized in *SI Appendix*, Fig. S3) but also the TH-regulating transcription factor Nurr1 (Fig. 3 *E* and *F*; double arrows in Fig. 3 *I*–*L*). Intermingled with the pSyn+/TH−/Nurr1− neurons, we found also cells that were double-positive for TH and pSyn but negative for Nurr1 (arrows in Fig. 3 *I*–*L*). Thus, at this early stage, a significant portion of the affected neurons in the pars compacta remained intact but in a dysfunctional state, linked to the reduced expression of TH and Nurr1. Interestingly, in many pSyn+/TH− neurons, the expression of the vesicular transporter VMAT2 was preserved (arrows in Fig. 3 *M*–*P*). Taken together, these findings suggest a possible sequence of early DA neuron dysfunction initiated by a loss of Nurr1 expression, followed by loss of TH and maintenance of VMAT2.

Transplanted hES Cell-Derived DA Neurons Survive and Mature into Subtype-Specific Dopaminergic Neurons Regardless of the Pathological Environment. The progressive PD-like pathology expressed in the SynFib-treated rats, as described above, offers an attractive model for studies on the performance of grafted DA neurons in a pathological environment that replicates aspects of inflammation, progressive cell death, and synucleinopathy seen in the human disease. For this purpose, we transplanted hESC-derived DA progenitors (12) into the striatum 8 wk after the combined α-syn/PFF injection into the nigra. We also transplanted a group of animals that were

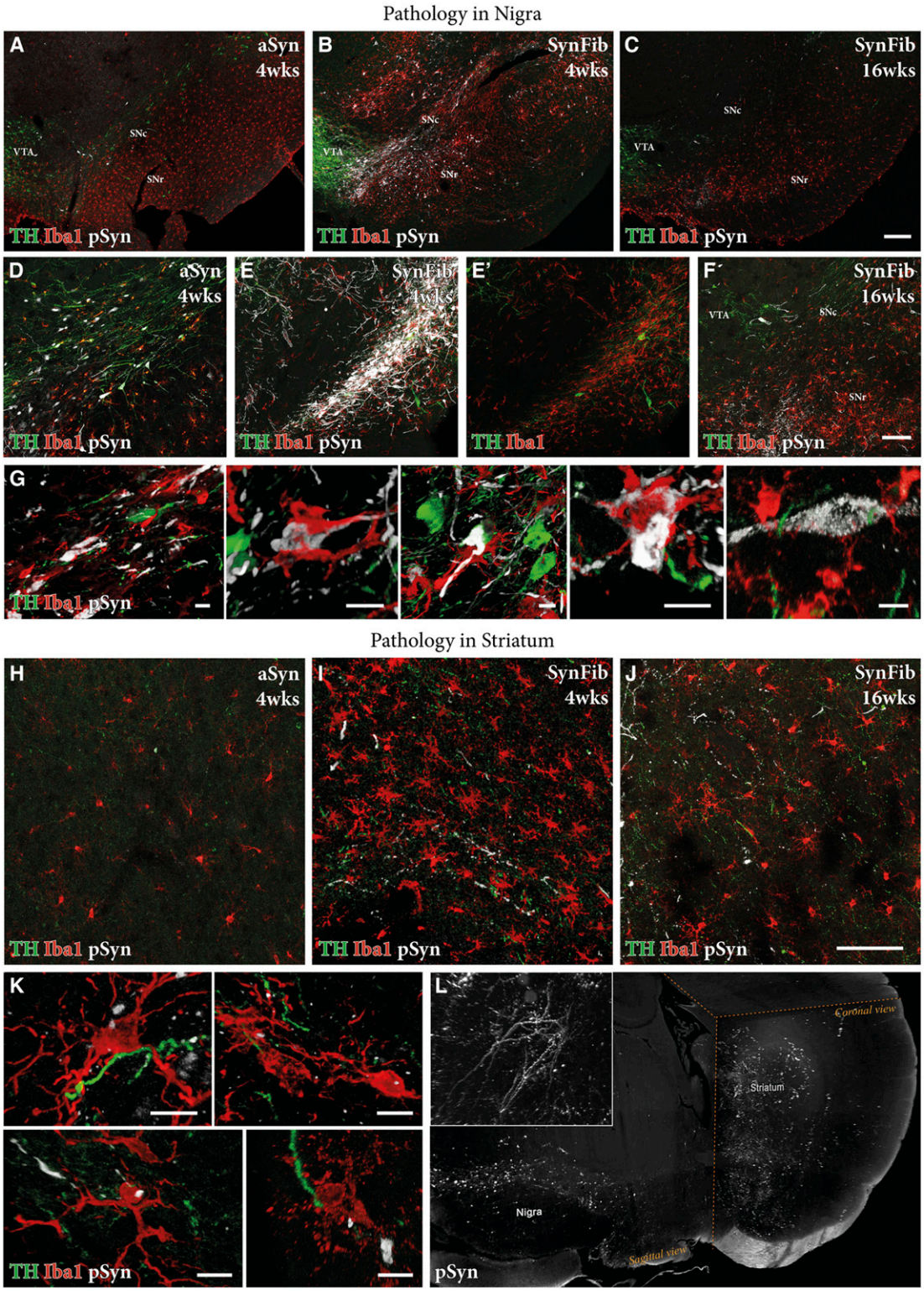

Fig. 2. Comparison of pSyn pathology and inflammation in the aSyn and SynFib models. Representative photographs of triple-stained nigral sections in the aSyn and SynFib groups show the presence of pSyn pathology (white), activated microglia (red), and TH loss (green) over time (*A*–*C*). Higher-magnification images of these are shown in *D*–*F*. Examples of colocalization of microglia to cell bodies containing pSyn pathology from SynFib 4-wk animals are shown in *G*. Representative photographs of the same staining combination in the striatum are shown in *H*–*J*. Microglia containing puncta of pSyn+ staining were observed in the striatum, examples of which from the SynFib 4-wk animals are shown in *K*. The level of pSyn host pathology is difficult to appreciate in two dimensions, although shown in *H*–*J*. We therefore performed iDISCO clearing and light-sheet microscopy to demonstrate the dense network of pSyn pathology in SynFib animals. A video of this whole-brain imaging is found in Movie S1, while a still image of this video is shown in *L*. SNc, substantia nigra pars compacta; SNr, substantia nigra pars reticulata; VTA, ventral tegmental area. (Scale bars, 200 μm [*A*–*C*], 100 μm [*D*–*F* and *H*–*J*], and 10 μm [*G* and *K*].)

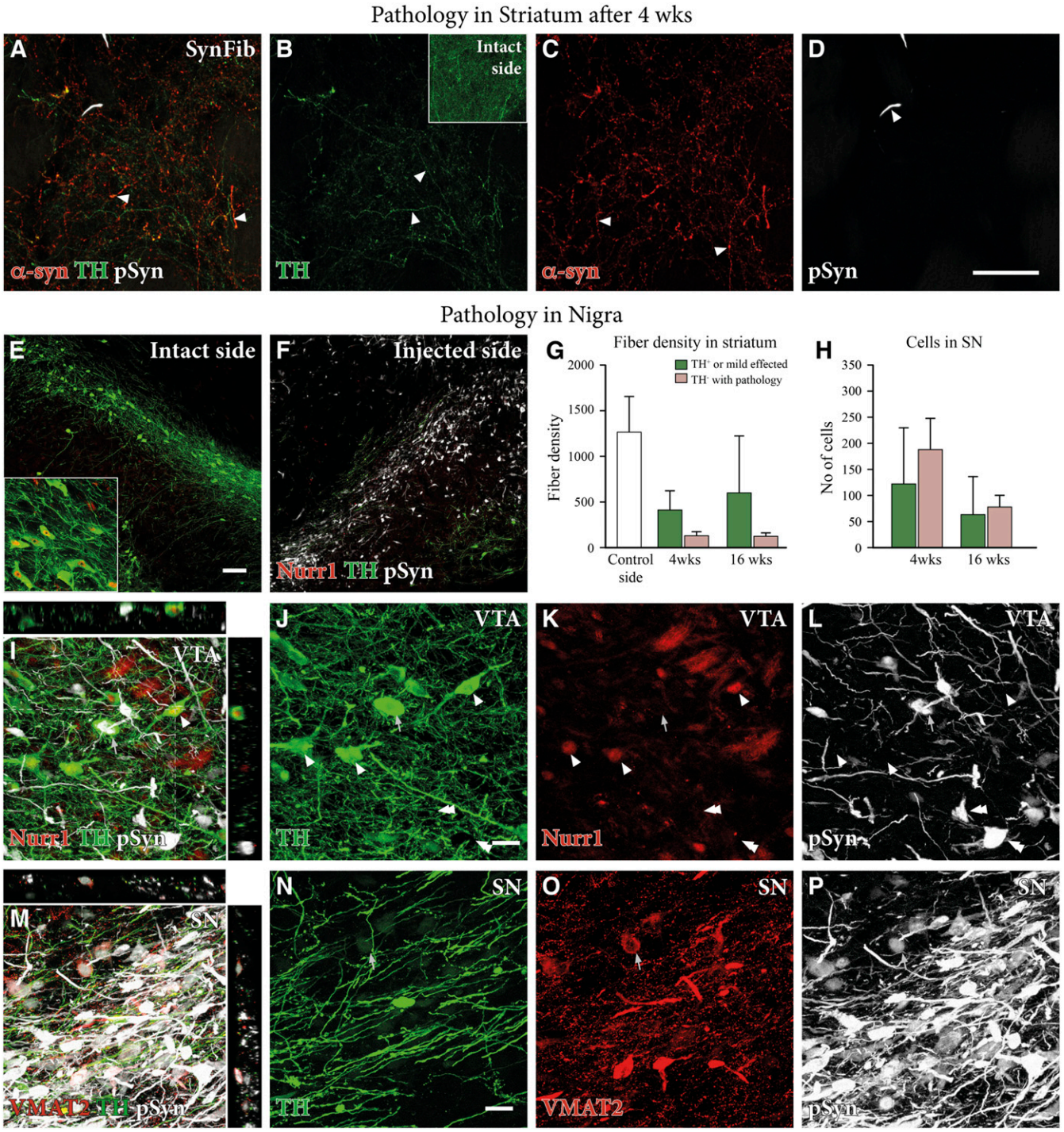

Fig. 3. Dopaminergic dysfunction and down-regulation in the SynFib model. Triple staining of striatal tissue for α-syn (red), TH (green), and pSyn (white) shown in *A*–*D* indicated that there were a number of TH−, α-syn+ fibers in the striatum, indicating TH down-regulation and quantified in *G* ($n = 6$ per group for 4 wk, $n = 5$ per group for 16 wk, and $n = 11$ for relative intact side controls). Triple staining of Nurr1 (red), TH (green), and pSyn (white) (*E* and *F*) also indicated down-regulation of TH in nigral cell bodies on the injected side, quantified in *H* ($n = 6$ per group for 4 wk and $n = 5$ per group for 16 wk). The same staining in the VTA is shown in high magnification in *I*–*L*, with arrowheads indicating TH+, Nurr1+, and pSyn− cells, and arrows indicating TH+, Nurr1−, and pSyn+ cells. VMAT (red), TH (green), and pSyn (white) triple staining of the SN is shown in high magnification in *M*–*P* with an arrow showing a TH+, VMAT+, and pSyn+ cell. All data are presented as mean ± SEM. (Scale bars, 50 μm [*A*–*D*], 100 μm [*E* and *F*], and 20 μm [*I*–*P*].)

partially lesioned with 6-OHDA using the same cell preparation. These animals served as a useful control, as the partial 6-OHDA lesion yields a similar degree of DA neuron degeneration but without the distinct pathological changes that are present in the SynFib model. When analyzing the grafts 6 wk after transplantation using an antibody recognizing human-specific neural cell-adhesion molecule (hNCAM), we found good graft survival and innervation of the surrounding host striatum in both groups (Fig. 4 *A* and *B*). Out of the transplanted rats, 4/4 in the 6-OHDA group and 5/5 in the SynFib group had surviving grafts (Fig. 4 *A* and *B*). Assessment

of graft size showed that the graft cores were of comparable size [$t_{(7)}$ =1.103, P = n.s.] (Fig. 4*C*). Analysis of graft-derived fiber outgrowth by three-dimensional mapping of the hNCAM-positive fibers (using the method described in ref. 34) showed that the grafted cells had a similar ability to extend their processes throughout the brain at this time point, including those areas normally innervated by the midbrain DA neurons (Fig. 4*D*). Additionally, we found no significant differences in terms of the fiber density or pattern of distribution in the SynFib-treated animals relative to the 6-OHDA controls. Despite slight variations in the size and placement of the grafts, the innervation patterns were notably consistent between grafted animals in the two groups (zoomed images in Fig. 4*D*). Thus, no differences in the graft outcome were observed despite the ongoing inflammatory and pathological environment of the striatum in the SynFib model at the time of transplantation.

Next, we assessed the potential impact of the host environment on the maturation of the transplanted hESC-derived DA progenitors at later time points after transplantation (12 and 18 wk). We found that, in both groups, the cells survived and matured to authentic DA neurons of the A9 and A10 subtypes, as indicated by the extensive expression of TH (Fig. 4 *E* and *F*) and TH/Girk2/Calbindin (Fig. 4 *I* and *J*), respectively, supported by the expression of the midbrain DA neuron marker Pitx3 (Fig. 4 *G* and *H*), indicating that the host environment did not affect the ability of the transplanted cells to undergo subtype-specific maturation in the host striatum.

Previous studies in our laboratory have shown the ability of transplanted hESC-derived DA neurons to establish extensive synaptic connectivity with the host brain in the 6-OHDA model (34–36). Here, we used monosynaptic rabies tracing to find out whether this is the case also in the SynFib model, and whether the ability of the grafted cells to establish extensive host-to-graft connectivity is influenced by the difference in the host environment seen in the two models. Using this tracing system, transplanted cells

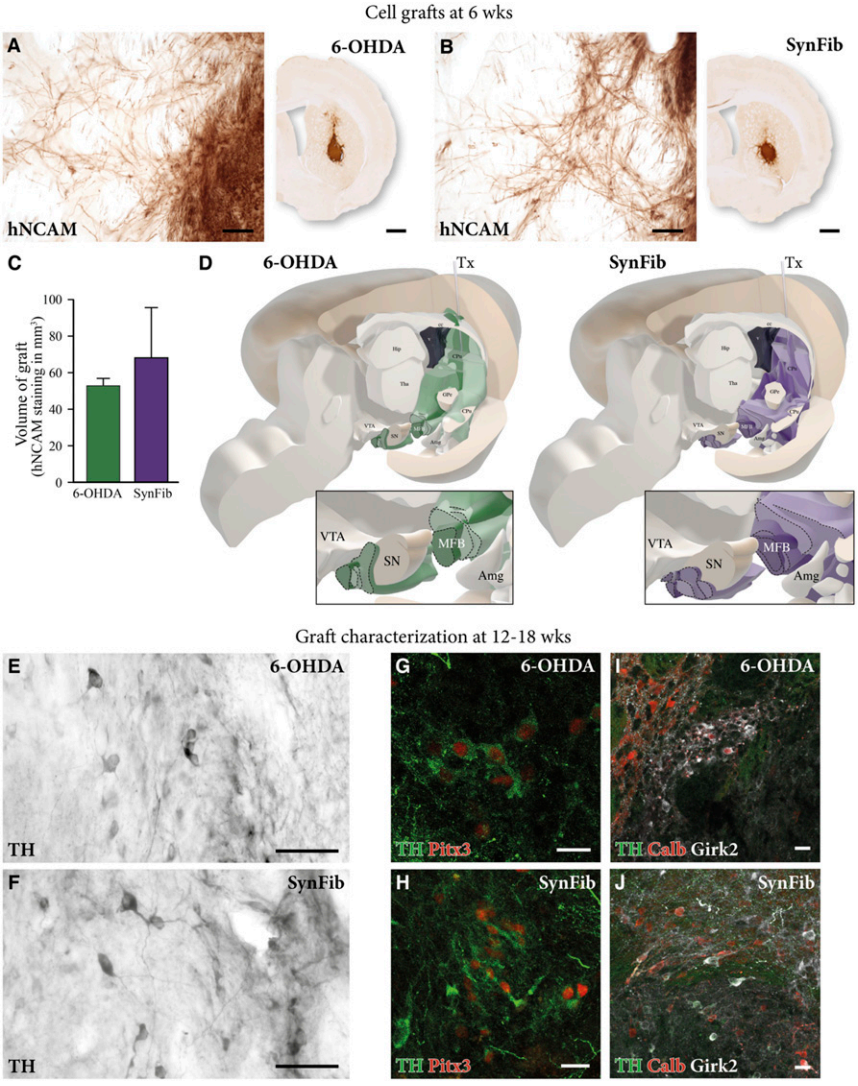

Fig. 4. hESC-derived DA transplant survival, innervation, and maturation in the SynFib model. hNCAM staining in *A* and *B* shows surviving grafts in both the 6-OHDA and SynFib models, and quantified and showing no significant difference in *C*. High magnification of this staining showing hNCAM innervation of the surrounding striatum is also shown in *A* and *B*. This hNCAM innervation was mapped throughout the brain in both models, the pattern and level of which are graphically depicted in *D*. High-magnification images indicating the maturation of grafts using TH in *E* and *F*, TH (green) and Pitx3 (red) in *G* and *H*, and TH (green), Calbindin (red), and Girk2 (white) in *I* and *J* are also shown. Amg, amygdala; cc, corpus collosum; GPe, globus pallidus; Hip, hippocampus; MFB, medial forebrain bundle; Tha, thalamus; Tx, transplant. All data are presented as mean ± SEM. (Scale bars, 1 mm and 50 μm in high magnification [*A* and *B*], 50 μm [*E* and *F*], and 20 μm [*G–J*].)

can be visualized by nuclear green fluorescent protein (GFP) expression (Fig. 5 *A*, *B*, and *D*, arrowheads), and cells that are infected with the modified rabies vector can be identified by the coexpression of both GFP and mCherry (Fig. 5 *A* and *B*). Similarly, host neurons making afferent connections with the transplanted cells will express mCherry. Since these cells do not express GFP, they can readily be identified as mCherry+/GFP− by microscope (Fig. 5*D*, arrows). Further spread of the modified rabies vector does not occur, as expression of the rabies glycoprotein is restricted to the transplanted neuron and therefore only first-order synapses are traced (37).

Fig. 5*C* shows the distribution of host neurons that provided input to the grafts in the SynFib-treated animals (*Bottom*) and the 6-OHDA lesioned controls (*Top*). The host connections originated in the same areas and further quantitative analysis showed that the traced neurons were similar in number in the two models (the degree of connectivity from the host region is indicated by the color chart in Fig. 5*C*). Neurons innervating the transplants were found in 11 host brain regions at 6 wk post-transplantation (Fig. 5*H*). In both groups, the local connections from the dorsolateral (DL) and medioventral (MV) striatum exhibit the highest connectivity ratio [Fig. 5*H*; caudate putamen (CPu) DL: 0.393 in 6-OHDA vs. 0.373 in SynFib animals; CPu MV: 0.221 in 6-OHDA vs. 0.371 in SynFib animals], followed by the motor cortex (Fig. 5*E*) and the thalamus (Fig. 5*G*). These results indicate that the pathological and inflammatory host environment present in the SynFib model had no negative influence on the ability of the transplanted cells to integrate anatomically into host striatal circuitry.

Significant Pathology Is Observed at the Site of Transplantation, with aSyn Inclusions Readily Detectable in a Small Number of TH+ Grafted Cells, Indicating Host-to-Graft Transfer of Pathology. We next sought to determine if there is any impact of the pathological environment specific to the SynFib model on the grafted cells, and to determine if potential spread of pathology to the grafted cells could be detected in the animals killed at 12 to 18 wk post-transplantation. The grafts were easily detected in the striatum based on the human-specific marker STEM121 (Fig. 6 *A* and *E*), and their cellular composition was similar, with areas rich in TH+ neurons occurring most commonly at the periphery of the grafts (Fig. 6 *C* and *G* in high magnification). Interestingly, in both groups, we found that there was an infiltration of microglia into the core of the grafts (Fig. 6 *B* and *F*). We have previously determined that the hESC-derived transplants do not generate any microglia (38), indicating that the microglia observed here are host-derived. When examined at higher magnification (Fig. 6 *D* and *H*), we found the microglia to be in a more activated state and present in higher numbers in the SynFib model than in the 6-OHDA lesioned animals, possibly indicating their involvement in patrolling the environment and scavenging pathology. Additionally, in the SynFib-grafted animals, the microglia were seen to contain small deposits of pSyn (Fig. 6*H*), a phenomenon that was absent in the 6-OHDA animals (Fig. 6*D*).

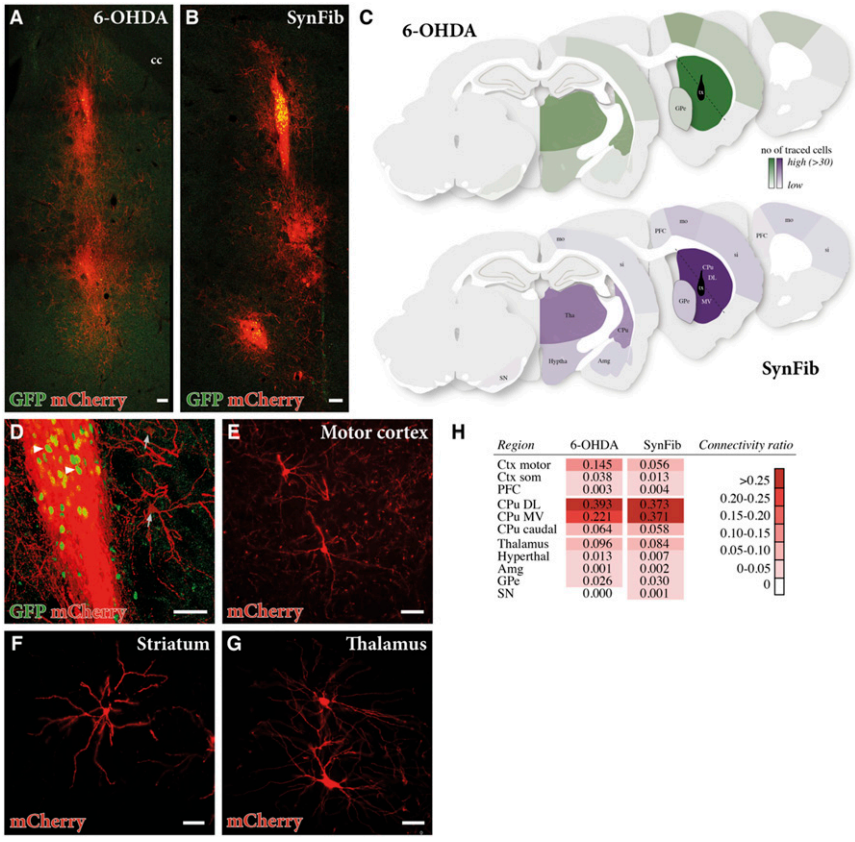

Fig. 5. Synaptic integration analysis of transplanted hESC-derived DA neurons. Double staining for GFP (green) and mCherry (red) shows the transplanted cells after rabies injection to assess the host integration of the grafted cells (*A* and *B*). GFP+/mCherry+ cells (arrowheads in *D*) show transplanted cells whereas GFP−/mCherry+ cells (arrows in *D*) show host neurons making synaptic connections with grafted cells. GFP−/mCherry+ were mapped and their number and location are graphically depicted in *C* where the darker the color, the greater the number of host-connecting neurons in that region. High-magnification images of individual mCherry+ host neurons from the areas of the brain most highly synaptically connected with the graft are shown in *E*–*G*. A connectivity ratio of the number of host connections relative to transplanted cells is depicted in *H*. Ctx, cortex; Hyptha, hypothalamus; mo, motor cortex; PFC, pre-frontal cortex; si, somatosensory cortex. (Scale bars, 100 μm [*A* and *B*] and 50 μm [*D*–*G*].)

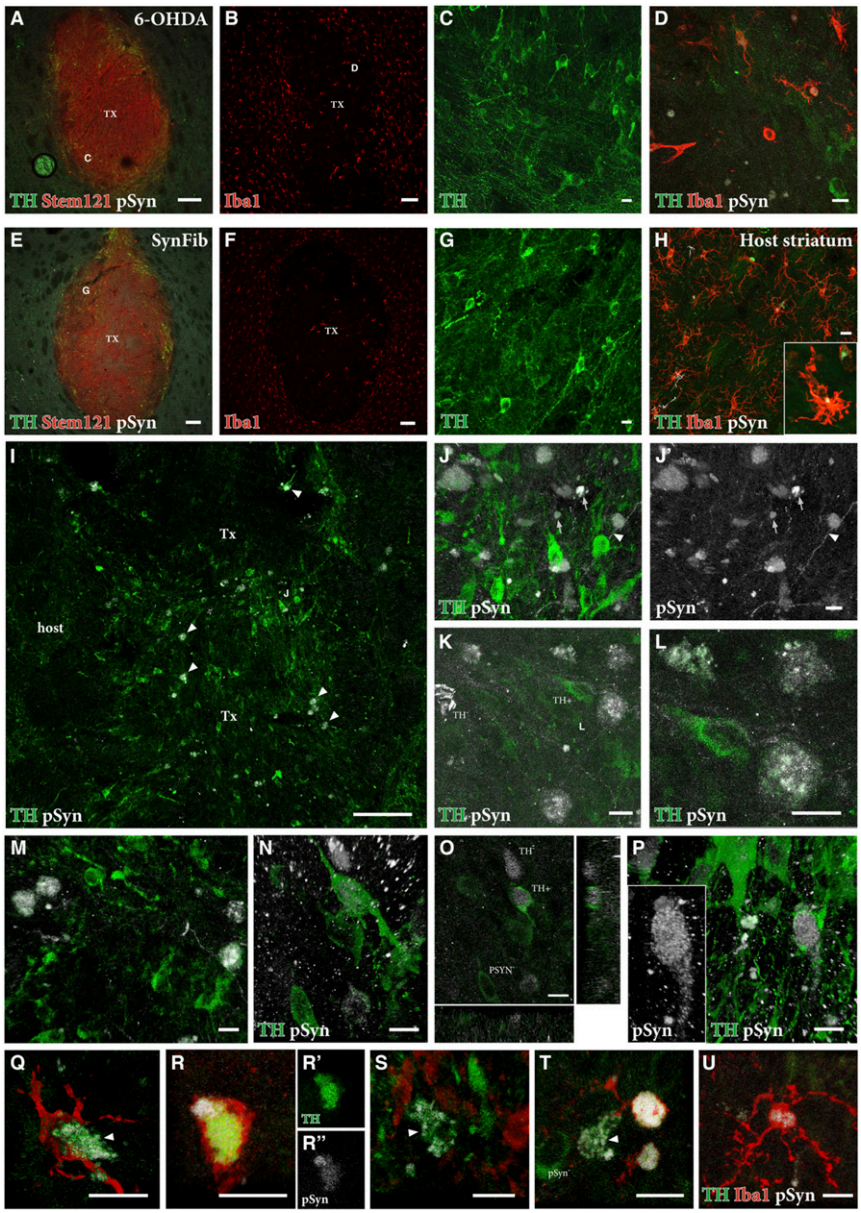

Fig. 6. pSyn pathology and inflammation in the grafted striatum. Triple staining of TH (green), Stem121 (red), and pSyn (white) is shown in *A* and *E* with high magnification of TH+ cells in the regions indicated shown in *C* and *G*. Iba1 (red) staining of graft cores is shown in *B* and *F* with high-magnification triple staining of TH (green), Iba1 (red), and pSyn (white) shown in *D–H*. The *Inset* in *H* is an Iba1+ cell containing pSyn+ puncta. Double staining of TH (green) and pSyn (white) is shown in *I–P* with arrowheads in *I* indicating double-positive cells, which can be seen more easily in high magnification (*J–P*). Arrowheads in *J* and *J′* indicate pSyn+ deposits were found within (mostly TH-negative) fibers, while arrows in *J* and *J′* indicate pSyn+ deposits extracellularly, outside the TH+ neurons. Double staining within grafted neurons is shown in *K–N* and *P* with an orthogonal view in *O*. Triple staining of TH (green), Iba1 (red), and pSyn (white) in *Q–U* shows the colocalization of activated microglia around TH+/pSyn+ cells in the graft core. (*C*) High magnification of area indicated in *A*; (*G*) High magnification of area indicated in *E*; (*D*) High magnification of area indicated in *B*. (Scale bars, 100 μm [*A*, *B*, *E*, *F*, and *I*] and 10 μm [*C*, *D*, *G*, *H*, and *J–U*].)

Upon examination of the SynFib-grafted animals using double immunostaining of TH and pSyn, we found numerous instances of colabeling within TH+ neurons in the graft core (indicated by arrowheads in Fig. 6*I*) but not in the 6-OHDA lesioned animals transplanted with the same cells. In addition, pSyn+ deposits were found within (mostly TH-negative) fibers (arrowheads in Fig. 6 *J* and *J′*), and extracellularly, outside the TH+ neurons, in structures that may represent distorted axons or cellular debris (arrows in Fig. 6 *J* and *J′*). To ensure that instances of double labeling of TH and pSyn (examples are shown in Fig. 6 *K–P*) were correctly assigned and located within the cell, we generated confocal *z* stacks of the double-labeled cells. The orthogonal images generated in this way confirmed the presence of pSyn within the cytoplasm (Fig. 6*O*), and in some cases also the nucleus (Fig. 6*P*), of grafted TH+ cells. pSyn containing TH+ neurons were found, albeit in low numbers, in all four SynFib grafts analyzed but absent in the 6-OHDA grafts. pSyn deposits were also found in cells lacking TH expression. Although the identity of these cells is unclear, it seems possible that a small proportion of pSyn+ DA neurons may have lost their TH expression due to down-regulation of TH, as observed in early-stage pathology in endogenous SN cells in this model (Fig. 6 *K* and *O*).

Finally, we asked the question whether the appearance of pSyn+ pathology in the grafted TH+ cells could be related to the increased presence of activated microglia in the grafts. In

areas of the graft containing pSyn+/TH+ cells, we observed pockets of Iba1+ microglia colocalized within that region, and found several instances where activated microglia occurred in close apposition to, or surrounding, the pSyn+/TH+ cells (Fig. 6 *Q*–*S*). The presence of pSyn+ deposits in some of these activated microglia provides further support for a role in the scavenging or destruction of pathological aggregates (Fig. 6 *T* and *U*).

Discussion

Pioneering trials where fetal VM tissue was transplanted into patients with PD have shown an important proof of concept that intrastriatal DA neuron transplants can restore DA transmission and mediate clinical improvements (1, 26). In line with clinical observations, post mortem analyses of transplanted brains have shown long-term (up to 24 y) graft survival and significant graft-derived innervation of the host brain (22). However, the post mortem analysis also showed evidence of Lewy body pathology in some of the transplants (17–23). Although the pathology observed has not been directly linked to diminished graft function, it is possible that the appearance of pathology in the transplant may compromise the function of the graft over time. However, the presence of pathology in the grafted cells, and indeed any potential impact that this may have on graft integrity, has been difficult to assess experimentally due to a lack of appropriate preclinical in vivo models.

The most common preclinical rodent model for assessing therapeutic/restorative cell- and gene-based interventions in PD is the 6-OHDA toxin model. This model results in the rapid death of DA neurons and significant motor impairment but does not recapitulate the characteristic pathological features of the disease, such as inflammation and synucleinopathy. A number of more disease-relevant models have been developed, including several transgenic mouse lines and aSyn overexpression rat models that better recapitulate these pathological features of PD (39, 40). However, the length of time these models take to develop pathology, coupled with the high variability in DA cell death and motor impairment, makes them less suitable for studies of long-term outcomes of cell transplantation (41). To overcome this hurdle, we have developed a model that combines overexpression of human α-syn (at a level that does not produce degeneration on its own) with delivery of preformed human α-syn fibrils. This model results in an accelerated development of pathology that progresses over time, accompanied by prominent axonal pathology and a progressive loss of nigral DA neurons. In this model, DA dysfunction and measurable motor impairment become apparent after only 4 wk. Inflammation has long since been implicated in the pathology of PD (30), and we found that microglia were activated and recruited to the areas of pSyn pathology, suggesting that inflammation is also present in the SynFib model generated here. The early activation of microglia observed in this model in response to the development of α-syn pathology is consistent with a role of activated microglia as an early indicator of neuropathological changes in PD (42).

The progressive time course is an attractive feature of this model, making it possible to distinguish between an early symptomatic stage that develops within the first month after vector injection, characterized by axonal pathology and down-regulation of both TH and Nurr1 in the pSyn+ DA neurons, and a later manifest stage that develops over the subsequent months, when a significant portion (>50%) of the nigral DA neurons have degenerated and part of the still-surviving neurons remain with the expression of pSyn+ pathology.

Importantly, we have demonstrated an early and stable motor impairment in at least 50% of the animals. This motor impairment was observed using two spontaneous and one drug-induced motor tests indicating a measurable motor impairment at a time when the pathology of the model is developing, thus providing the opportunity to interfere with the subsequent pathological process and prevent the ultimate cell death. Due to the progressive nature of the model and the fact that the pathology develops within a relatively short time, a therapeutic time window is opened in which to assess interventions such as cell-replacement therapy.

When using this model to assess the survival, maturation, integration, and integrity of hESC-derived DA cells after transplantation into the ongoing pathological and degenerative environment that develops in this model, we found no significant effect on the grafts: The survival and size of the grafts were similar in the SynFib and the standard toxin models, and the same extensive fiber outgrowth and afferent host connectivity were seen in both models. At later time points, however, 12 to 18 wk postgrafting, we observed marked differences in two disease-related pathological changes, namely the presence of pSyn+ inclusions and aggregates and the increased numbers and size of activated glia that occurred in the SynFib-treated animals but not in the toxin model.

At 6 wk posttransplantation, we found an increased incidence of pSyn+ deposits in the grafts. However, given that grafted cells at this time point are still relatively immature, it was difficult to determine if the pSyn staining observed was due to host pathology infiltrating the graft tissue or whether the pathology was actually within grafted cells. Thus, we proceeded to look at a number of animals at 12, 15, or 18 wk after transplantation, at a stage when the DA neurons are phenotypically mature although not yet functionally mature (12). Indeed, we found TH+/pSyn+ cells in all SynFib animals that we examined, and in none of the 6-OHDA animals. Confocal microscopy of double-stained sections showed unequivocally that the pSyn-stained inclusions were located in the cytoplasm, and in some cases also the nucleus, of the TH+ neurons. While this occurred in all grafts in the SynFib group, it is important to note that the appearance of this pSyn pathology was still a relatively rare event and seen in only a small percentage of the TH+ neurons. We also found a small number of grafted cells that were TH−/pSyn+. These cells were found clustered around other TH+ cells and thus may potentially be dopaminergic neurons that had down-regulated TH; however, it is also possible that this signifies the presence of pathology in nondopaminergic grafted cells. Previous studies have shown the spread of α-syn to grafts of rat fetal VM DA neurons transplanted in the AAV-α-syn overexpression model (43–45). These studies, however, did not observe the phosphorylated pathological form of α-syn, pSyn, in grafted neurons, and the mismatch of species, that is, overexpression of high levels of human aSyn in combination with rat fetal tissue grafts, may not be optimal for studies of this kind. Oligomeric or protofibrillar α-syn is able to transfer between cells, as seen both in cell culture and in the brain (46–48), but it has been shown that the seeding and development of pSyn pathology are more efficient when the PFFs and the monomeric α-syn are from the same species (49). Therefore, our study of α-syn host-to-graft transfer utilizes a humanized model where both the α-syn and the grafted cells are human, and where the α-syn expression is closer to physiological levels, in order to replicate the clinical setting as closely as possible.

Microglia are known to be activated by α-syn aggregates and oligomers, and they are also the primary cells to clear extracellular α-syn (50, 51), indicating that they may be involved in the α-syn–triggered pathological process as well as in the removal of toxic α-syn species (see ref. 52 for a review). Consistent with this view, we observed activated microglia in areas of pSyn+ pathology within the graft, in some cases closely apposed to pSyn+ DA neurons, and we also observed cases where microglial cells were seen to engulf TH+/pSyn+ cells and processes. Microglia have been proposed to act as a mediator of α-syn–induced toxicity in midbrain DA neurons (51), and a recent study has suggested that they may play a protective role in the transfer of α-syn pathology to grafted cells (44). However, this protective

role is brought into question when, in the George et al. study (44), the transfer of pathology was increased by activation of the microglia with lipopolysaccharide. This suggests an alternative possibility, namely that microglia may play an active role in the transfer process, triggered by the release of α-syn oligomers or aggregates from the dystrophic and degenerating nigrostriatal axons present in the pathological environment surrounding the grafted cells. This possibility is strengthened by the fact that cell-released α-syn has been shown to act as an agonist for TLR2 receptors through which microglia become neurotoxic (53) and recently published post mortem data showing that microglial activation in fetal DA-grafted patients actually precedes the α-syn pathology in grafted cells, indicating that activated microglia may play a role in the propagation and spread of α-syn pathology (54).

In summary, we have developed a humanized and accelerated α-syn model that recapitulates many of the cardinal features of PD. The pathology develops within a short time frame, rendering it suitable for long-term assessment of therapeutic interventions such as cell-replacement therapy. We show that hESC-derived DA neurons, transplanted into the pathological environment present in the SynFib-treated animals, survive, mature, and innervate the host brain just as well as in the standard toxin model, with the same extensive integration into host striatal circuitry. However, we have also shown, as a result of the pathology present in this model system, the appearance of pathological pSyn+ inclusions in grafted dopaminergic cells, mimicking what has been observed in some of the PD patients receiving transplants of fetal tissue. While as yet we do not know the long-term consequences of the presence of pathology in grafted neurons, the humanized and accelerated xenograft model developed herein provides unique possibilities to do so. In addition, future cell-based therapies for PD may be based on autologous grafting using the patient's own cells to prevent graft rejection by the immune system and mitigating the need for immunosuppressive drug therapy. This raises the question, however, whether cells derived from reprogrammed patient cells may be inherently more vulnerable to the disease process than cells from healthy donors. The humanized α-syn model described here may provide the opportunity to assess to what extent cells from different patient groups, for example, sporadic or genetic causes, are more vulnerable to the pathological host environment. Such studies would be valuable for the preclinical evaluation of the suitability of patient-derived cells for cell-replacement therapy in the clinic.

Materials and Methods

Animals. The studies were performed in accordance with the European Union Directive (2010/63/EU) and approved by the local ethical committee for the use of laboratory animals and the Swedish Department of Agriculture (Jordbruksverket). Female Sprague–Dawley rats (225 to 250 g; Charles River Germany) were housed with ad libitum access to food and water under a 12-h light/dark cycle.

Experimental Design. The rats were injected with either AAV-α-syn or AAV-α-syn combined with PFFs at two sites in the substantia nigra. For the transplant studies, animals received either unilateral AAV-α-syn combined with PFF injection, as above, or an intrastriatal 6-OHDA lesion, and were immunosuppressed with daily injections of ciclosporin (10 $mg \cdot kg^{-1} \cdot d^{-1}$, intraperitoneally; Apoteksbolaget) to prevent graft rejection, starting 2 d prior to transplantation and continuing until the end of the experiment. All animals received a unilateral striatal cell transplantation of hESC-derived DA cells at 8 wk and were perfused between 6 and 18 wk later. hESC-derived DA cells containing the rabies helper constructs were used for monosynaptic rabies tracing. These animals received an injection of EnvA-pseudotyped ΔG mCherry rabies to the graft site 5 wk after transplant and were perfused 7 d later.

Animals used for establishing the SynFib model: aSyn alone 4 wk ($n = 6$), aSyn alone 16 wk ($n = 6$), SynFib 4 wk ($n = 8$), SynFib 16 wk ($n = 16$), and SynFib 12 wk for iDISCO analysis ($n = 4$). Animals used for transplant study: 6-OHDA + transplant 6 wk ($n = 12$, $n = 8$ used for rabies tracing), 6-OHDA + transplant 12 to 18 wk ($n = 4$), SynFib + transplant 6 wk ($n = 16$, $n = 10$ used for tracing), and SynFib + transplant 12 to 18 wk ($n = 4$).

AAV and Fibril Production. An AAV6 vector expressing human wild-type α-syn under the human synapsin-1 promoter was used in this study, as described (55). The viral titer was 4.7×10^{14} genome copies/mL, used at a working dilution of 10 to 20%. Human α-syn PFFs (5 μg/μL) were prepared from full-length recombinant human α-syn, as described (56).

hESC Differentiation. RC-17 hESCs differentiated into dopaminergic ventral mesencephalically patterned progenitors according to a standardized protocol known to generate functionally mature DA neurons after 5 to 6 mo in vivo (10, 12, 34, 57) were used in all experiments (described in detail in ref. 12). RC-17 hESCs expressing the rabies helper construct (generated by lentiviral infection as described in ref. 34) were used for monosynaptic rabies tracing.

Rabies Virus Production. EnvA-pseudotyped ΔG-rabies was produced as described in ref. 36. Vector titers were 20 to 30×10^6 transducing units/mL. A working dilution of 5% was used for experiments.

Surgery. Surgery was performed under general anesthesia using a solution of fentanyl and medetomidine (20:1) (Apoteksbolaget). Animals were secured in a stereotaxic frame with the tooth bar adjusted to the flathead position. For aSyn animals, 4 μL 10% AAV-α-syn was injected unilaterally into the SN at two sites (anteroposterior [A/P] −5.3, M/L −1.6, D/V −7.2 and A/P −5.3, M/L −2.6, D/V −6.7). For SynFib animals, 4 μL of a mixture of 20% AAV-α-syn and 5 μg/μL sonicated α-syn PFFs (to yield a final concentration of 10% AAV-α-syn and 2.5 μg/μL) was injected unilaterally into the SN at two sites (A/P −5.3, M/L −1.6, D/V −7.2 and A/P −5.3, M/L −2.6, D/V −6.7). All injections were made at a rate of 0.2 μL/min, and the needle was left in place for 2 min before being slowly removed. 6-OHDA (3.5 μg/μL, free base) was injected at a rate of 1 μL/min at two sites in the striatum (A/P −0.5, M/L −2.5, D/V −5.0 and A/P +0.5, M/L −4.2, D/V −5.0), 2.8 μL per site.

For cell-transplantation surgery (at 8 wk postlesion), 4 μL of cell suspension containing 75,000 cells per microliter was unilaterally injected at four sites into the striatum (A/P +0.5, M/L −3.0, D/V −5.5/−4.5 and A/P +1.2, M/L −2.6, D/V −5.5/−4.5) (1 μL per site) at a rate of 1 μL/min. Animals with transplants of hESC-derived DA neurons containing rabies helper construct received 4 μL ΔG-rabies at the same four sites (1 μL per site) at a rate of 1 μL/min.

Behavioral Analysis. Behavioral tests were performed at 4 and 16 wk postlesion by the same researcher, blind to the rats' treatment group.

Test of forelimb akinesia was performed as described previously (58). The number of steps taken by the left and right paws when passively moved along a 90-cm trajectory was recorded in forehand and backhand directions. Rats were trained to complete the test 1 d prior to testing. To avoid bias, the median of 3 consecutive days was used. Forelimb use in the cylinder test was completed as described previously (59). The number of forelimb paw touches against the wall of the glass cylinder was counted until a total of 20 had been performed, and the percentage of touches made with the left paw (contralateral side) was recorded. Amphetamine-induced rotation (2.5 mg/kg; Apoteksbolaget) was recorded over 90 min using an automated system as previously described (60). Data were expressed as net full body turns per minute toward the lesion side.

Immunohistochemistry. Rats were transcardially perfused under sodium pentobarbitone anesthesia with 0.9% saline solution followed by ice-cold 4% paraformaldehyde (PFA). The brains were postfixed for 24 h in 4% PFA, incubated in 25% sucrose for 48 h, and sectioned using a freezing microtome to a thickness of 35 μm in a 1:8 series. Immunohistochemistry was performed on free-floating sections after incubation in Tris-ethylenediaminetetraacetate for 30 min at 80 °C for antigen retrieval. Staining was performed as previously described (61), using antibodies listed in *SI Appendix*, Fig. S4. Tyramide signal amplification (TSA) was used as described (62) to increase the detection of Nurr1-positive cell bodies. Following incubation in ABC solution (VECTASTAIN Elite ABC-HRP Kit, PK-6100) for 30 min, the sections were treated with biotinyl tyramide (1:2,500 in K-phosphate-buffered saline (PBS) containing 0.009% H_2O_2) for 30 min and labeled by a 2-h incubation with fluorophore-conjugated streptavidin (1:500).

Bright-field images were captured at low magnification using a flatbed scanner (Epson Perfection V850 PRO) and an Olympus AX microscope. Fluorescence imaging was performed with a Leica DMI6000B microscope

and a Leica SP8 confocal microscope. Three-dimensional images were generated from *z* stacks of pictures captured from 35-μm-thick sections using Volocity v.5.4.2 software (PerkinElmer). Stitching of images was performed in Figs. 2 *A*–*C*, 5 *A* and *B*, and 6 *A*, *B*, *E*, and *F*).

Light-Sheet Microscopy. A proportion of SynFib animals ($n = 4$, 12 wk postinjection) were processed for light-sheet microscopy using the iDISCO clearing method (63). Animals were perfused with 2% PFA and the brains were postfixed on ice for 1 h, transferred to PBS, and divided by a midline sagittal cut, allowing each hemisphere to be processed individually. Processing was performed as previously described (35), using mouse polyclonal anti-pSyn81A (1:1,000) as the primary antibody, and Alexa Fluor 647-conjugated donkey anti-mouse (1:750) as the secondary antibody. The cleared hemispheres were imaged on an Ultra Microscope II (LaVision Biotec) equipped with an sCMOS camera (Andor Neo model 5.5-CL3) using a 1.3× objective lens (LaVision LVMI-Fluor 1.3×/0.08 MI Plan) and 680/30 emission for Alexa Fluor 647. Stacks were acquired with ImspectorPro64 (LaVision Biotec) using 5-μm *z* steps. Stacks were taken with 10% overlap and stitched using Arivis Vision 4D 3.01 software. Rendered movies were compiled in Final Cut Pro-10.4.3 (Apple).

Densitometry. TH+ fiber density was measured bilaterally at three sites in the medial, central, and lateral parts of the striatum, expressed as a percentage of the intact side. The optical density readings were corrected for background density, as measured from unstained areas of the same sections. Analysis was performed blind, the images were converted to 8-bit black and white within ImageJ, and the mean gray value was recorded.

Stereology. DA neuron loss in the substantia nigra pars compacta (SNpc) was quantified by unbiased stereological estimations of the TH+ cells using the optical fractionator principle (64). A count was performed on every eighth section (section sampling fraction = 8) covering the full extent of the SNpc, yielding seven or eight sections per animal for analysis. The average mounted section thickness (height) was 20 μm and no guard zones were implemented. Stereo Investigator software (MBF Bioscience) was used with a Leitz DMRBE microscope. Regions of interest were traced using a 5× objective and counting was performed using a 100× oil-immersion objective. A maximal coefficient error of 0.08 was accepted for cells to be counted. Analysis was performed blind and data were expressed as a percentage of the intact side.

Graft Volume Quantification. To determine graft volume, photomicrographs of striatal sections containing an hNCAM+ cell core were taken, and ImageJ was calibrated using a graticule image by associating the number of pixels with a known distance. The area of the graft in each striatal section was determined in a 1 in 8 series using the ImageJ freehand drawing tool and the graft volume was assessed according to Cavalieri's principle, given the known distance between each section and the known section thickness (65).

Graphical Representation of Graft Innervation and Synaptic Integration. For representation of graft fiber outgrowth, an entire 1:8 series of hNCAM 3,3′-diaminobenzidine (DAB)-stained sections was scanned and images corresponded to the matching coronal section from the Paxinos and Watson rat brain atlas (66). The area of hNCAM+ fiber outgrowth was mapped onto each anatomical plane. For the representation of host synaptic inputs to the graft, the process was repeated with mCherry DAB-stained sections.

Statistics. Behavioral and immunohistochemical data were analyzed using a one-way ANOVA followed by a post hoc Bonferroni test or unpaired Student's *t* test where appropriate. Results were deemed statistically significant if $P < 0.05$. All data are expressed as mean ± SEM. Representative images were chosen based on extensive confocal sampling of the material available, with the number of sampling regions based on 63× magnification in the *z* stack. Fig. 2: $n = 9$ animals, 2 to 8 sampling regions per animal; Fig. 3: $n = 3$ animals, 5 to 8 sampling regions per animal; Fig. 6: $n = 6$ animals, 3 to 30 sampling regions per animal.

Data Availability. All data supporting the findings of this study are available within the article and its *SI Appendix*.

ACKNOWLEDGMENTS. We thank Michael Sparrenius and Jenny G. Johansson for excellent technical assistance, Andrew Adler for help with immunohistochemical staining and TSA amplification, and Thomas Perlmann for the kind gift of the Pitx3 antibody. The research received funding from the New York Stem Cell Foundation, European Research Council (ERC) under ERC Grant Agreement 771427, Swedish Research Council (2016-00873), Swedish Parkinson Foundation (Parkinsonfonden), Swedish Brain Foundation, Strategic Research Area at Lund University Multipark, and Knut and Alice Wallenberg Stiftelse (KAW 2018-0040). S.S. is funded by the European Union Horizon 2020 Programme (H2020-MSCA-ITN-2015) under the Marie Skłodowska-Curie Innovative Training Network and Grant Agreement 676408. M.P. is a New York Stem Cell Foundation Robertson Investigator.

1. A. Björklund, O. Lindvall, Replacing dopamine neurons in Parkinson's disease: How did it happen? *J. Parkinsons Dis.* **7** (suppl. 1), S21–S31 (2017).
2. O. Lindvall *et al.*, In reply: Fetal brain grafts and Parkinson's disease. *Science* **250**, 1435 (1990).
3. R. A. Barker, J. Barrett, S. L. Mason, A. Björklund, Fetal dopaminergic transplantation trials and the future of neural grafting in Parkinson's disease. *Lancet Neurol.* **12**, 84–91 (2013).
4. R. A. Barker; TRANSEURO consortium, Designing stem-cell-based dopamine cell replacement trials for Parkinson's disease. *Nat. Med.* **25**, 1045–1053 (2019).
5. Y. Chen *et al.*, Chemical control of grafted human PSC-derived neurons in a mouse model of Parkinson's disease. *Cell Stem Cell* **18**, 817–826 (2016).
6. D. Doi *et al.*, Isolation of human induced pluripotent stem cell-derived dopaminergic progenitors by cell sorting for successful transplantation. *Stem Cell Reports* **2**, 337–350 (2014).
7. P. J. Hallett *et al.*, Successful function of autologous iPSC-derived dopamine neurons following transplantation in a non-human primate model of Parkinson's disease. *Cell Stem Cell* **16**, 269–274 (2015).
8. G. Hargus *et al.*, Differentiated Parkinson patient-derived induced pluripotent stem cells grow in the adult rodent brain and reduce motor asymmetry in parkinsonian rats. *Proc. Natl. Acad. Sci. U.S.A.* **107**, 15921–15926 (2010).
9. T. Kikuchi *et al.*, Human iPS cell-derived dopaminergic neurons function in a primate Parkinson's disease model. *Nature* **548**, 592–596 (2017).
10. A. Kirkeby *et al.*, Generation of regionally specified neural progenitors and functional neurons from human embryonic stem cells under defined conditions. *Cell Rep.* **1**, 703–714 (2012).
11. S. Kriks *et al.*, Dopamine neurons derived from human ES cells efficiently engraft in animal models of Parkinson's disease. *Nature* **480**, 547–551 (2011).
12. S. Nolbrant, A. Heuer, M. Parmar, A. Kirkeby, Generation of high-purity human ventral midbrain dopaminergic progenitors for in vitro maturation and intracerebral transplantation. *Nat. Protoc.* **12**, 1962–1979 (2017).
13. Center for iPS Cell Research and Application (CiRA), Kyoto University, Announcement of physician-initiated clinical trials for Parkinson's disease (2018). www.cira.kyoto-u.ac.jp/e/pressrelease/news/180730-170000.html. Accessed 24 August 2018.
14. D. Normile, First-of-its-kind clinical trial will use reprogrammed adult stem cells to treat Parkinson's. *Science*, 10.1126/science.aau9466 (2018).
15. UMIN Kyoto trial to evaluate the safety and efficacy of iPSC-derived dopaminergic progenitors in the treatment of Parkinson's disease (UMIN, 2018). https://upload.umin.ac.jp/cgi-open-bin/ctr_e/ctr_view.cgi?recptno=R000038278. Accessed 21 December 2018.
16. R. A. Barker, M. Parmar, L. Studer, J. Takahashi, Human trials of stem cell-derived dopamine neurons for Parkinson's disease: Dawn of a new era. *Cell Stem Cell* **21**, 569–573 (2017).
17. J. H. Kordower *et al.*, Fetal nigral grafts survive and mediate clinical benefit in a patient with Parkinson's disease. *Mov. Disord.* **13**, 383–393 (1998).
18. J. H. Kordower *et al.*, Neuropathological evidence of graft survival and striatal reinnervation after the transplantation of fetal mesencephalic tissue in a patient with Parkinson's disease. *N. Engl. J. Med.* **332**, 1118–1124 (1995).
19. J. H. Kordower *et al.*, Long-term fetal nigral graft-survival and putamenal innervation correlates with functional recovery in a patient with Parkinsons-disease—A clinical-pathological analysis. *Exp. Neurol.* **135**, 166 (1995).
20. J. Y. Li *et al.*, Lewy bodies in grafted neurons in subjects with Parkinson's disease suggest host-to-graft disease propagation. *Nat. Med.* **14**, 501–503 (2008).
21. J. Y. Li *et al.*, Characterization of Lewy body pathology in 12- and 16-year-old intrastriatal mesencephalic grafts surviving in a patient with Parkinson's disease. *Mov. Disord.* **25**, 1091–1096 (2010).
22. W. Li *et al.*, Extensive graft-derived dopaminergic innervation is maintained 24 years after transplantation in the degenerating parkinsonian brain. *Proc. Natl. Acad. Sci. U.S.A.* **113**, 6544–6549 (2016).
23. I. Mendez *et al.*, Cell type analysis of functional fetal dopamine cell suspension transplants in the striatum and substantia nigra of patients with Parkinson's disease. *Brain* **128**, 1498–1510 (2005).
24. D. Kirik *et al.*, Parkinson-like neurodegeneration induced by targeted overexpression of alpha-synuclein in the nigrostriatal system. *J. Neurosci.* **22**, 2780–2791 (2002).
25. R. L. Klein, M. A. King, M. E. Hamby, E. M. Meyer, Dopaminergic cell loss induced by human A30P alpha-synuclein gene transfer to the rat substantia nigra. *Hum. Gene Ther.* **13**, 605–612 (2002).
26. C. Lo Bianco, J. L. Ridet, B. L. Schneider, N. Deglon, P. Aebischer, Alpha-synucleinopathy and selective dopaminergic neuron loss in a rat lentiviral-based model of Parkinson's disease. *Proc. Natl. Acad. Sci. U.S.A.* **99**, 10813–10818 (2002).
27. N. P. Visanji *et al.*, α-Synuclein-based animal models of Parkinson's disease: Challenges and opportunities in a new era. *Trends Neurosci.* **39**, 750–762 (2016).
28. K. Albert *et al.*, Downregulation of tyrosine hydroxylase phenotype after AAV injection above substantia nigra: Caution in experimental models of Parkinson's disease. *J. Neurosci. Res.* **97**, 346–361 (2019).

29. P. Thakur *et al*., Modeling Parkinson's disease pathology by combination of fibril seeds and α-synuclein overexpression in the rat brain. *Proc. Natl. Acad. Sci. U.S.A.* **114**, E8284–E8293 (2017).
30. P. L. McGeer, S. Itagaki, B. E. Boyes, E. G. McGeer, Reactive microglia are positive for HLA-DR in the substantia nigra of Parkinson's and Alzheimer's disease brains. *Neurology* **38**, 1285–1291 (1988).
31. Y. Chu, J. H. Kordower, Age-associated increases of alpha-synuclein in monkeys and humans are associated with nigrostriatal dopamine depletion: Is this the target for Parkinson's disease? *Neurobiol. Dis.* **25**, 134–149 (2007).
32. M. Decressac *et al*., α-Synuclein-induced down-regulation of Nurr1 disrupts GDNF signaling in nigral dopamine neurons. *Sci. Transl. Med.* **4**, 163ra156 (2012).
33. J. H. Kordower *et al*., Disease duration and the integrity of the nigrostriatal system in Parkinson's disease. *Brain* **136**, 2419–2431 (2013).
34. T. Cardoso *et al*., Target-specific forebrain projections and appropriate synaptic inputs of hESC-derived dopamine neurons grafted to the midbrain of parkinsonian rats. *J. Comp. Neurol.* **526**, 2133–2146 (2018).
35. A. F. Adler *et al*., hESC-derived dopaminergic transplants integrate into basal ganglia circuitry in a preclinical model of Parkinson's disease. *Cell Rep.* **28**, 3462–3473.e5 (2019).
36. S. Grealish *et al*., Monosynaptic tracing using modified rabies virus reveals early and extensive circuit integration of human embryonic stem cell-derived neurons. *Stem Cell Reports* **4**, 975–983 (2015).
37. R. Etessami *et al*., Spread and pathogenic characteristics of a G-deficient rabies virus recombinant: An in vitro and in vivo study. *J. Gen. Virol.* **81**, 2147–2153 (2000).
38. K. Tiklová *et al*., Single cell gene expression analysis reveals human stem cell-derived graft composition in a cell therapy model of Parkinson's disease. bioRxiv:10.1101/720870 (5 August 2019).
39. P. Jiang, D. W. Dickson, Parkinson's disease: Experimental models and reality. *Acta Neuropathol.* **135**, 13–32 (2018).
40. L. A. Volpicelli-Daley, D. Kirik, L. E. Stoyka, D. G. Standaert, A. S. Harms, How can rAAV-α-synuclein and the fibril α-synuclein models advance our understanding of Parkinson's disease? *J. Neurochem.* **139** (suppl. 1), 131–155 (2016).
41. A. Ulusoy, D. A. Di Monte, α-Synuclein elevation in human neurodegenerative diseases: Experimental, pathogenetic, and therapeutic implications. *Mol. Neurobiol.* **47**, 484–494 (2013).
42. M. G. Tansey, M. S. Goldberg, Neuroinflammation in Parkinson's disease: Its role in neuronal death and implications for therapeutic intervention. *Neurobiol. Dis.* **37**, 510–518 (2010).
43. E. Angot *et al*., Alpha-synuclein cell-to-cell transfer and seeding in grafted dopaminergic neurons in vivo. *PLoS One* **7**, e39465 (2012).
44. S. George *et al*., Microglia affect α-synuclein cell-to-cell transfer in a mouse model of Parkinson's disease. *Mol. Neurodegener.* **14**, 34 (2019).
45. C. Hansen *et al*., α-Synuclein propagates from mouse brain to grafted dopaminergic neurons and seeds aggregation in cultured human cells. *J. Clin. Invest.* **121**, 715–725 (2011).
46. K. C. Luk *et al*., Pathological α-synuclein transmission initiates Parkinson-like neurodegeneration in nontransgenic mice. *Science* **338**, 949–953 (2012).
47. W. Peelaerts *et al*., α-Synuclein strains cause distinct synucleinopathies after local and systemic administration. *Nature* **522**, 340–344 (2015).
48. L. A. Volpicelli-Daley *et al*., Exogenous α-synuclein fibrils induce Lewy body pathology leading to synaptic dysfunction and neuron death. *Neuron* **72**, 57–71 (2011).
49. K. C. Luk *et al*., Molecular and biological compatibility with host alpha-synuclein influences fibril pathogenicity. *Cell Rep.* **16**, 3373–3387 (2016).
50. H. J. Lee, J. E. Suk, E. J. Bae, S. J. Lee, Clearance and deposition of extracellular alpha-synuclein aggregates in microglia. *Biochem. Biophys. Res. Commun.* **372**, 423–428 (2008).
51. W. Zhang *et al*., Aggregated alpha-synuclein activates microglia: A process leading to disease progression in Parkinson's disease. *FASEB J.* **19**, 533–542 (2005).
52. V. Sanchez-Guajardo, N. Tentillier, M. Romero-Ramos, The relation between α-synuclein and microglia in Parkinson's disease: Recent developments. *Neuroscience* **302**, 47–58 (2015).
53. C. Kim *et al*., Neuron-released oligomeric α-synuclein is an endogenous agonist of TLR2 for paracrine activation of microglia. *Nat. Commun.* **4**, 1562 (2013).
54. C. W. Olanow, M. Savolainen, Y. Chu, G. M. Halliday, J. H. Kordower, Temporal evolution of microglia and α-synuclein accumulation following foetal grafting in Parkinson's disease. *Brain* **142**, 1690–1700 (2019).
55. M. Decressac *et al*., GDNF fails to exert neuroprotection in a rat α-synuclein model of Parkinson's disease. *Brain* **134**, 2302–2311 (2011).
56. L. A. Volpicelli-Daley, K. C. Luk, V. M. Lee, Addition of exogenous α-synuclein preformed fibrils to primary neuronal cultures to seed recruitment of endogenous α-synuclein to Lewy body and Lewy neurite-like aggregates. *Nat. Protoc.* **9**, 2135–2146 (2014).
57. S. Grealish *et al*., Human ESC-derived dopamine neurons show similar preclinical efficacy and potency to fetal neurons when grafted in a rat model of Parkinson's disease. *Cell Stem Cell* **15**, 653–665 (2014).
58. M. Olsson, G. Nikkhah, C. Bentlage, A. Björklund, Forelimb akinesia in the rat Parkinson model: Differential effects of dopamine agonists and nigral transplants as assessed by a new stepping test. *J. Neurosci.* **15**, 3863–3875 (1995).
59. T. Schallert, S. M. Fleming, J. L. Leasure, J. L. Tillerson, S. T. Bland, CNS plasticity and assessment of forelimb sensorimotor outcome in unilateral rat models of stroke, cortical ablation, parkinsonism and spinal cord injury. *Neuropharmacology* **39**, 777–787 (2000).
60. U. Ungerstedt, G. W. Arbuthnott, Quantitative recording of rotational behavior in rats after 6-hydroxy-dopamine lesions of the nigrostriatal dopamine system. *Brain Res.* **24**, 485–493 (1970).
61. M. Decressac, B. Mattsson, M. Lundblad, P. Weikop, A. Björklund, Progressive neurodegenerative and behavioural changes induced by AAV-mediated overexpression of α-synuclein in midbrain dopamine neurons. *Neurobiol. Dis.* **45**, 939–953 (2012).
62. J. C. Adams, Biotin amplification of biotin and horseradish peroxidase signals in histochemical stains. *J. Histochem. Cytochem.* **40**, 1457–1463 (1992).
63. N. Renier *et al*., iDISCO: A simple, rapid method to immunolabel large tissue samples for volume imaging. *Cell* **159**, 896–910 (2014).
64. M. J. West, H. J. Gundersen, Unbiased stereological estimation of the number of neurons in the human hippocampus. *J. Comp. Neurol.* **296**, 1–22 (1990).
65. Y. Garcia, A. Breen, K. Burugapalli, P. Dockery, A. Pandit, Stereological methods to assess tissue response for tissue-engineered scaffolds. *Biomaterials* **28**, 175–186 (2007).
66. G. Paxinos, C. Watson, *The Rat Brain in Stereotaxic Coordinates*, (Academic Press, London, UK, ed. 5, 2005).